Conformational Polymorphism on Imatinib Mesylate: Grinding Effects

DAMIÁN GRILLO,[1] GRISELDA POLLA,[1] DANIEL VEGA[1,2]

[1]Departamento Física de la Materia Condensada, Gerencia de Investigación y Aplicaciones, Comisión Nacional de Energía Atómica, San Martín, Buenos Aires, Argentina

[2]Escuela de Ciencia y Tecnología, Universidad Nacional de General San Martín, Campus Miguelete, Edificio Tornavías, San Martín, Buenos Aires, Argentina

Received 13 May 2011; revised 11 August 2011; accepted 7 September 2011

Published online 4 October 2011 in Wiley Online Library (wileyonlinelibrary.com). DOI 10.1002/jps.22772

ABSTRACT: Crystal structures of polymorphs α and β of imatinib mesylate were obtained. Thermal behavior and grinding effects were studied by X-ray powder diffraction and differential scanning calorimetry techniques. Molecules in forms α and β exhibit significant conformational differences due to dissimilar intramolecular interactions, which stabilize their molecular conformations. In spite of that, both crystal structures present a dimer-chain arrangement. Dimers are mainly determined by hydrogen bonding interactions and some weak π–π interactions. Connections between dimers are provided by mesylate ions to determine chains of dimers. Neighboring chains are linked by very weak interactions: C—H···π interactions in form α and π–π interactions in form β. At room temperature, thermal disorder was observed in the mesylate ion in form α, which could be removed at low temperatures (–123°C). Form β was found to be the more stable form at room temperature. Both polymorphs exhibit a tendency to generate amorphous material by grinding, which can be converted to a crystalline phase by either temperature or aging. When amorphous crystallization is kinetically studied at room temperature, form β is obtained after a week. Conversely, when the crystallization is activated by temperature, the final obtained crystal form depends on the starting material, proving the importance of seeding. J Pharm Sci 101:541–551, 2012
Keywords: polymorphism; crystal structure; milling; amorphous; X-ray powder diffractometry; solid state stability; thermal analysis

INTRODUCTION

Organic compounds can crystallize in more than one crystal form.[1] The ability of a substance to exist in several different forms is known as polymorphism. If crystals of pharmaceuticals exhibit polymorphism, their physical properties such as density, melting point, solubility and stability, bioavailability, and processability will be dependent on the crystal form.[2] Moreover, these properties can be subjected to change when thermodynamic variables like pressure or temperature are modified.[3] The importance of polymorphism knowledge for pharmaceutical industry lies on having reliable and robust processes.[4,5]

Among different processes to suffer by drug substances, they can be subjected to particle size reduction, grinding, and compression before they are finally blended with excipients to produce the final formulation. The milling process results in a reduction in the particle size of a given material. This procedure can lead to either a polymorphic conversion or to generation of an amorphous substance.[6] On one hand, the formation of a high-energy amorphous material is usually undesirable in that it must be metastable and, given the opportunity, will spontaneously transform to crystalline material.[6] On the other hand, the energy changes that take place during polymorphic phase transformations (first-order transitions) require modifications in the bonding scheme among molecules in the structure and, sometimes, changes in molecular conformation. The process can be imagined as first requiring a loosening of the bonding configuration in the initial crystal, transformation to a

Correspondence to: Daniel Vega (Telephone: +54-11-6772-7107; Fax: +54-11-6772-7121; E-mail: vega@cnea.gov.ar)

Journal of Pharmaceutical Sciences, Vol. 101, 541–551 (2012)

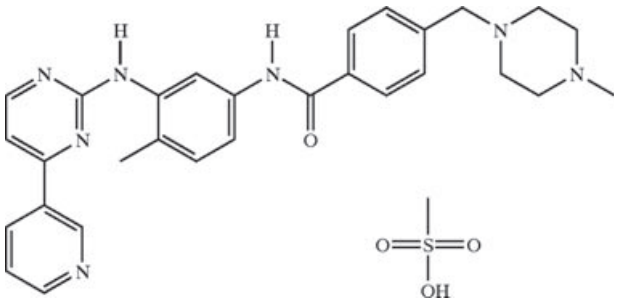

Figure 1. Drawing of imatinib mesylate molecule.

high-energy intermediate form, and then a recrystallization out of chaos.[7]

Some illuminating examples of conversions such as described above can be found in literature.[8,9] For example, the milling process of cimetidine enables conversions of forms B and C to form A, whereas form A transforms into form D only upon nucleation. In all cases, the particle size reduction step resulted in substantial formation of an amorphous phase.[10]

Following our program on studying polymorphism on pharmaceuticals,[11,12] our attention was focused on imatinib {4-[(4-methylpiperazin-1-yl)methyl]-N-[4-methyl-3-[(4-pyridin-3-ylpyrimidin-2-yl)amino]-phenyl]benzamide}, a drug used to treat certain types of cancer. It is currently marketed as its mesylate salt. Imatinib mesylate (see Fig. 1), a tyrosine kinase inhibitor, is one of the first molecularly targeted therapies to have been used in the clinic. It has proven to be efficient in the treatment of chronic myeloid leukemia, gastrointestinal stromal tumors, and also in other malignancies that involve expression of a tyrosine kinase.[13,14]

Imatinib mesylate exhibits polymorphism. Several crystalline forms and amorphous material are described.[15] Among them, crystalline forms α and β can be found as the more frequent polymorphs. In particular, form α was described as metastable (and hygroscopic) at room temperature and was then initially indicated as not useful for the preparation of pharmaceutical preparations.[16] In spite of the previously mentioned studies, physical characterizations of crystalline and amorphous phases are still incomplete. The aim of the present work is to provide a complete solid-state characterization. At first, we focused our work on the study of single crystal structures of forms α and β, describing intermolecular bonding scheme, a first step to understand the ability to produce amorphous material by grinding. Subsequently, we have provided a thermal characterization of isolated crystalline forms, mixtures, and milled mixtures to recognize the thermal behavior of forms α and β and different transformations provided by the same amorphous material. Finally, we have introduced some thermodynamic arguments to support both the proposed stability relation and the role played by the amorphous phase based on the above mentioned ideas.

EXPERIMENTAL

Methods

X-ray powder diffraction (XRPD) patterns were recorded on an X'Pert Philips PW3020 diffractometer (Philips, Almelo, the Netherlands) over a 2θ range of 3°–40° using graphite monochromatized Cu Kα radiation (1.54184 Å), in aluminum sample holders at room temperature (1° divergence slit; 1° detector slit and 0.1 mm receiving slit, 0.02° scanning step, 2 s counting time.). In order to remove the preferred orientation, the crystalline material was ground in a manual agate mortar (1 g sample, 5 min grinding time), then suitable samples for XRPD measurement were obtained.

Single-crystal X-ray diffraction data were collected both at room temperature and at $T = -123$°C using a Gemini A diffractometer (Oxford Diffraction, Blacksburg, Virginia). Data-collection strategy and data reduction followed standard procedures implemented in CrystAlisPro software.[17]

The structures were solved using program SHELXS-97[18] and refined using the full-matrix LS procedure with SHELXL-97.[18] Anisotropic displacement parameters were employed for non-hydrogen atoms, and H atoms were treated isotropically with $U_{iso} = 1.2$ (for those attached to aromatic carbons and the N atom) or 1.5 times (for those bonded to methyl carbons) the equivalent displacement parameter (U_{eq}) of the parent atoms. All H atoms were located at the expected positions and were refined using a riding model. In the final cycle of refinement, LS weights of the form $w = 1/[\sigma^2(F_o^2) + (a \times P)^2 + b \times P]$, where $P = [(F_o^2) + 2 \times F_c^2)]/3$, were employed. Routines employed to create crystallographic information files were from WinGX package.[19]

Crystallographic data (excluding structure factors) for both crystal forms and both temperatures have been deposited in the Cambridge Crystallographic Data Centre[20] as supplementary publication numbers CCDC 821868, 821869, 821870, and 821871.

Differential scanning calorimetry (DSC) was carried out with a Shimadzu DSC-60 instrument (Shimadzu, Kyoto, Japan). Samples weighing 2–4 mg were heated in opened aluminum pans at a rate of 10°C/min under a nitrogen gas flow of 30 mL/min.

Slurry conversion experiment was performed with a Decalab hot stage (Decalab SRL, Buenos Aires, Argentina) with programmable temperature control. A suspension of 850 mg sample of form α with little amount of form β in 120 mL of isopropanol was placed in the hot stage, stirring it and varying its temperature in a controlled way between 29°C and 35°C in

Table 1. Crystal and Refinement Data for Forms α and β ($T = -123^{\circ}C$)

	Form α	Form β
Chemical formula	$C_{29}H_{32}N_7O^+ \cdot CH_3SO_3^-$	
Formula weight	589.72	
Temperature	–123°C	
Crystal system	Triclinic	
Space group	P-1	
Unit cell dimensions		
	a = 9.3362 (6) Å	a = 9.1093 (2) Å
	b = 9.8621 (6) Å	b = 10.4639 (2) Å
	c = 18.0236 (6) Å	c = 15.0699 (2) Å
	α = 81.298 (4)°	α = 93.457 (1)°
	β = 90.019 (4)°	β = 93.613 (1)°
	γ = 63.106 (8)°	γ = 90.389 (1)°
Volume	1458.54 (14) Å^3	1430.90 (5) Å^3
Z	2	2
Density (calculated)	1.3428 (2) g cm^{-3}	1.3687 (1) g cm^{-3}
Radiation, wavelength	Mo Kα, 0.71073 Å	Mo Kα, 0.71073 Å
Absorption coefficient	0.160 mm^{-1}	0.163 mm^{-1}
$F(000)$	624	624
Crystal size	0.30 × 0.06 × 0.03 mm^3	0.50 × 0.30 × 0.10 mm^3
θ range for data collection	3.53°–25.00°	3.86°–26.37°
Index ranges	$-11 \le h \le 11, -11 \le k \le 10, -21 \le l \le 21$	$-11 \le h \le 11, -13 \le k \le 13, -18 \le l \le 18$
Reflections collected	9157	37843
Observed reflections [$I > 2\sigma(I)$]	2200	4744
Independent reflections	5117	5856
Internal consistency	$R_{int} = 0.0608$	$R_{int} = 0.0317$
Refinement method	Full matrix on F^2	
Data/restraints/parameters	5117/0/379	2151/0/379
Goodness-of-fit on F^2	0.744	1.010
Final R indices [$I > 2\sigma(I)$]	$R_1 = 0.0459$, $wR_2 = 0.0627$	$R_1 = 0.0333$, $wR_2 = 0.0893$
R indices (all data)	$R_1 = 0.1388$, $wR_2 = 0.0747$	$R_1 = 0.0438$, $wR_2 = 0.0920$
Largest difference peak and hole	0.260, –0.262 eÅ^{-3}	0.445, –0.491 eÅ^{-3}

cycles of 1 h. After 5 days, the excess of solid was removed and dried at room temperature to be analyzed by XRPD.

Ultraviolet–visible (UV–Vis) absorbance was measured using a Lambda 25 UV/Vis spectrometer (PerkinElmer, Waltham, Massachusetts) in the range 200–800 nm using a quartz recipient with an optical pathway of 1 cm. Saturated solutions of forms α and β were obtained by placing an excess amount of sample in 1-propanol. The suspensions were stirred for 2 h at room temperature in capped glass vials. The solutions were filtered using 0.2-μm Millipore filter (Millipore, Billerica, Massachusetts)) and analyzed after appropriate dilution.

RESULTS AND DISCUSSION

Structural Analysis

Crystal structures of forms α and β were solved both at room temperature and at $T = -123^{\circ}C$. As will be discussed later, one of the room-temperature structure exhibits disorder, and single-crystal data and refinement details at–123°C are shown in Table 1. Selected torsional angles are listed in Table 2. Geometrical descriptions of relevant interactions are detailed in Table 3 (form α) and Table 4 (form β).

Each polymorph crystallizes in the space group P-1 with one molecule in asymmetric unit, as shown in Figures 2 and 3. These molecules exhibit quite different conformations. The main conformational differences are evident when inspecting C5—C4—C6—N2, C11—C10—N4—C9, and C11—C12—N5—C17 torsional angle values in Table 2. Analyzing the structural results, molecules in each crystal form are subjected to different intramolecular interactions to stabilize their molecular conformation. Although in form α a weak intramolecular hydrogen bond is determined by C11—H11···O1, giving a + *Syn-Periplanar* character to C11–C12–N5–C17, this interaction is not

Table 2. Selected Torsional Angles ($T = -123^{\circ}C$, Angles in °)

Torsional Angles	Form α	Form β
C3—C4—C6—C7	36.6 (6)	13.2 (2)
N3—C9—N4—C10	–27.1 (5)	–176.3 (1)
C11—C10—N4—C9	77.9 (4)	113.3 (2)
C11—C12—N5—C17	18.2 (4)	–51.8 (2)
C18—C17—N5—C12	176.4 (2)	–179.0 (1)
N5—C17—C18—C19	–25.8 (4)	–35.3 (2)
C20—C21—C24—N6	43.5 (4)	–23.7 (2)
O1—C17—C18—C23	–24.2 (4)	–33.5 (2)

Table 3. Geometrical Description of Relevant Interactions for Polymorph α (T =–123°C, Distances in Å, Angles in °)

Hydrogen Bond Interactions Donor—H···Acceptor	D—H	H···A	D···A	D—H···A
N4—H4···O4[a]	0.86	2.06	2.877(3)	159
N5—H5A···N3[b]	0.86	2.34	3.186(4)	168
N7—H7A···O2	0.91	1.89	2.790(4)	172
N7—H7A···O3	0.91	2.57	3.158(3)	123
C11—H11···O1 (intra)	0.93	2.24	2.816(4)	119
π–π Interactions				
Ring–Ring	Cg–Cg Distance	Distance Between Planes	Slippage	
Cg2—Cg2[b]	4.442(2)	3.222(1)	3.057	
C—H···π Interactions				
C—H···Ring	H···Cg	C—Cg	C—H···Cg	
C8—H8···Cg3[c]	2.94	3.702(3)	141	

[a]Symmetry code: (x, $1+y$,$-1+z$).
[b]Symmetry code: ($1-x$, $1-y$, $1-z$).
[c]Symmetry code: (x, $1+y$, z).

observed in form β and C11 –C12–N5–C17 exhibits a – *Syn-Clinal* character. Consequently, meanwhile a weak intramolecular hydrogen bond determined by C5—H5···N2 stabilizes form β and gives a + *Syn-Periplanar* character to C5–C4–C6–N2, this interaction is absent in form α and the torsion angle has a + *Syn-Clinal* character.

In both polymorphs, non-aromatic C1–C2–C3–C4–C5–N1 and C6–C7–C8–N3–C9–N2 (labeled as Cg1) rings are planar, whereas N6–C25–C26–N7–C27–C28 ring presents a chair conformation with puckering parameters Q = 0.584(3) Å, $\theta = 2.6(3)^\circ$, and $\phi = 5(7)^\circ$ in form α, and $Q = 0.581(2)$ Å, $\theta = 6.0(1)^\circ$, and $\phi = 15(2)^\circ$ in form β.

Crystal cohesion is provided mainly by intermolecular hydrogen bonding interactions, but there are other weak interactions that provide extra cohesion as well (see Tables 3 and 4). For both polymorphs, the crystal packing can be described as chains of dimers (see Figure 4 and 5).

In form α, each molecule in the dimer is linked to the other one through hydrogen bonds between N5 and N3; the dimer cohesion is also supported by the presence of a weak π–π interaction between the Cg2 rings (see Fig. 4). The dimers are connected between them via mesylate ions, which provide, on one hand, a hydrogen bond between N4 and O4 and, on the other hand, a bifurcated hydrogen bond joining N7 with O2 and O3 (the interaction with O2 is stronger than with O3). Cohesion between neighboring chains is provided by a very weak C—H···π interaction between C8 and Cg3 ring (see Fig. 4).

In form β the dimer is determined as a result of stronger hydrogen bond between N1 and N5 and weaker π–π interaction between the Cg2 rings that provide further cohesion to the dimer (see Fig. 5). As same as in form α, the connection between dimers is also supported by the mesylate ion, providing, on one hand, a hydrogen bond between N4 and O4, and between N7 and O2, on the other hand. Neighboring chains are linked through a weak π–π interaction between the Cg1 rings (see Table 4).

It is worth mentioning that at room temperature, form α is able to exhibit disorder. The mesylate ion in the crystal structure was modeled as a disordered one, with three different positions for each O atom and C atom in the ion. However, the disorder is not present at low temperatures (T =–123°C). The observed thermal disorder in the mesylate ion is the evidence that the bonding scheme among molecules (mainly among

Table 4. Geometrical Description of Relevant Interactions for Polymorph β (T =–123°C, Distances in Å, Angles in °)

Hydrogen Bond Interactions Donor—H···Acceptor	D—H	H···A	D···A	D—H···A
N4—H4···O4[a]	0.86	2.63	3.240(2)	130
N5—H5A···N1[b]	0.86	2.09	2.905(2)	158
N7—H7A···O2	0.91	1.95	2.831(2)	163
C5—H5···N2	0.93	2.35	2.717(2)	103
π–π Interactions				
Ring–Ring	Cg–Cg Distance	Distance Between Planes	Slippage	
Cg2—Cg2[b]	4.6215(8)	3.2650(6)	3.271	
Cg1—Cg1[c]	4.9795(8)	3.4876(6)	3.554	

[a]Symmetry code: ($1-x$, $1-y$, $1-z$).
[b]Symmetry code: ($-x$, $1-y$, $2-z$).
[c]Symmetry code: ($-x$,$-y$, $2-z$).

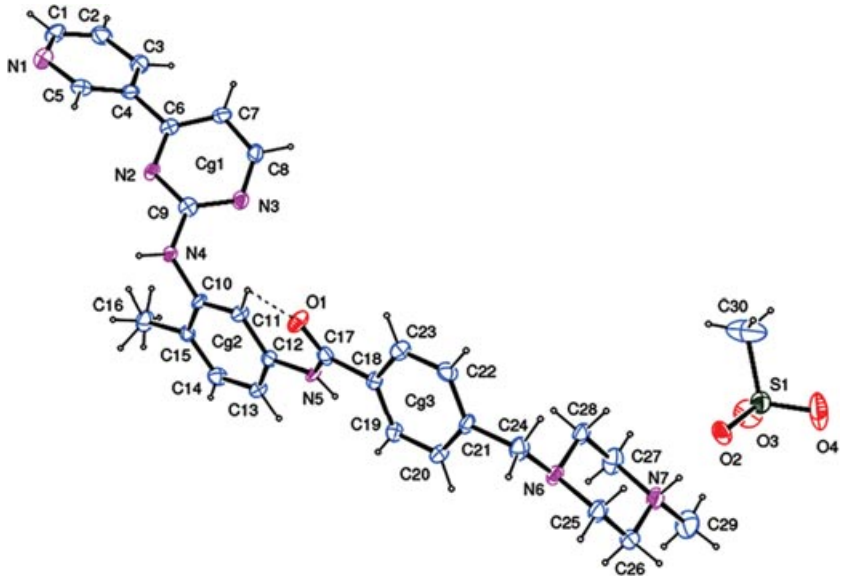

Figure 2. Representation of the molecule of imatinib mesylate form α showing the numbering scheme used and displacement ellipsoids drawn at 50% probability level. Intramolecular interactions are shown as dashed lines.

the nearest neighbors of dimers) is becoming weaker at room temperature, providing a substantial degree of molecular mobility.

A comparison between the calculated and observed XRPD diagrams for each crystalline form is shown in Figure 6. Calculated XRPD were performed with the disordered model obtained at room temperature. Inspecting Figure 6, preferred orientation effects are present in experimental patterns for both crystal forms. A 5-min grinding seemed to be enough for removing these effects, and a good correspondence can be observed between the calculated XRPD patterns obtained from X-ray single-crystal structural models and ground bulk material ones.

Stability Studies: Slurry Conversion and Relative Solubility by UV–Vis Absorbance

A powder crystalline sample composed of 850 mg of form α and a small amount of form β was subjected to a slurry conversion process for 5 days (see details in the *Methods* section). The solid sample remaining after the process was identified by XPRD as corresponded to form β, as shown in Figure 7. This result gives the evidence that the more stable polymorph in

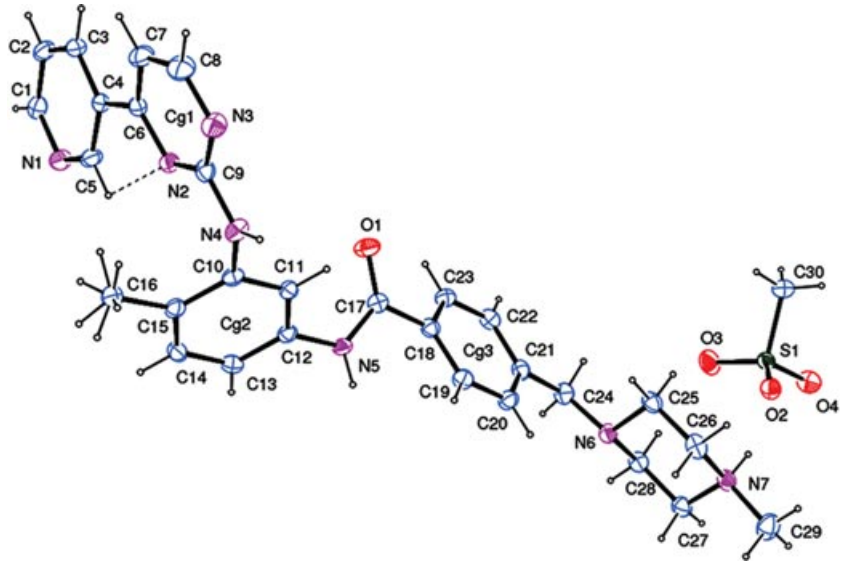

Figure 3. Representation of the molecule of imatinib mesylate form β showing the numbering scheme used and displacement ellipsoids drawn at 50% probability level. Intramolecular interactions are shown as dashed lines.

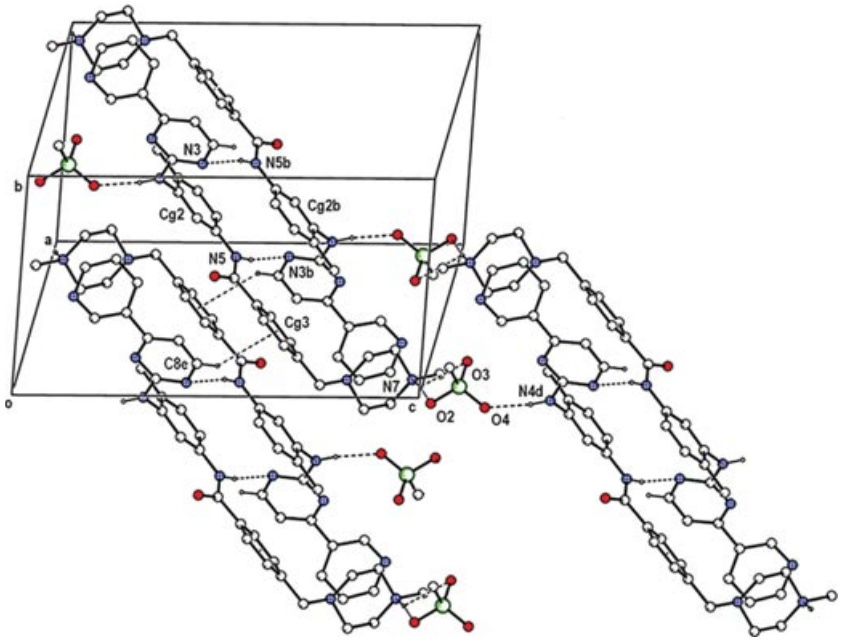

Figure 4. Packing diagram of imatinib mesylate form α showing relevant intermolecular interactions as dashed lines. Symmetry code b: $(1-x, 1-y, 1-z)$, symmetry code d: $(x,-1+y, 1+z)$, symmetry code e: $(x,-1+y, z)$.

this range of temperature corresponds to form β. In order to confirm this statement, the relative solubility was obtained by determining the UV–Vis spectra of an adequately diluted sample of saturated solutions for both as-grown polymorphs. Figure 8 shows that form α resulted as 2.5 times more soluble than form β, pointing out that form β is the more stable one.

Thermal Studies

As-grown samples of forms α and β were characterized by DSC, showing only one thermal event each (an endothermic peak), none of which are related to weight loss (as checked by thermogravimetric analysis). These transitions are related to the melting point for each crystal form (checked by visual inspection under hot-stage microscopy), with melting point $T_{onset} = 226^{\circ}C$ and heat of fusion $\Delta H_f = 105$ J/g for polymorph α (see Fig. 9 and Table 5) and $T_{onset} = 217^{\circ}C$ and $\Delta H_f = 110$ J/g for polymorph β (see Fig. 10 and Table 5).

The grinding effect on as-grown samples was also explored, not only because milling as-grown samples had been necessary to perform XRPD studies, but also because grinding will be a usual practice in any manufacturing process. After milling, both ground forms exhibit new thermal events. Figures 9 and 10 show the presence of an exothermic peak around $T = 140^{\circ}C$ for both ground forms before the corresponding melting points are reached. Moreover, the melting points changed from 226°C to 223°C and from 216°C to 213°C for forms α and β, respectively.

The crystal forms are conserved because the observed XRPD patterns (see Fig. 6) do not change and no other extra crystalline phase appears as a consequence of the grinding processes of forms α and β.

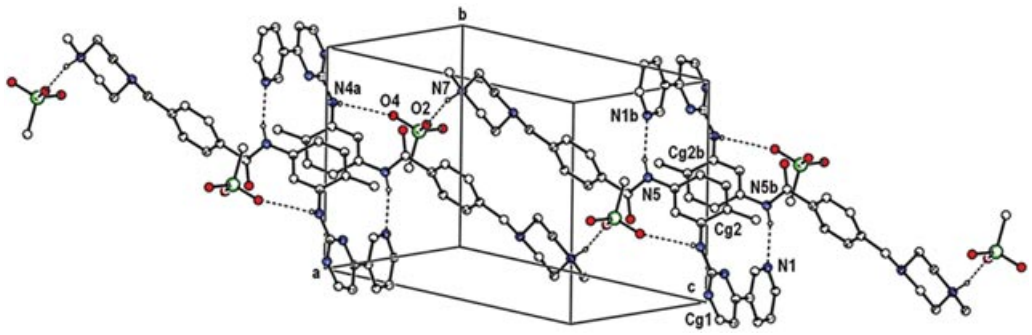

Figure 5. Packing diagram of imatinib mesylate form β showing relevant intermolecular interactions as dashed lines. Symmetry code a: $(1-x, 1-y, 1-z)$, symmetry code b: $(-x, 1-y, 2-z)$.

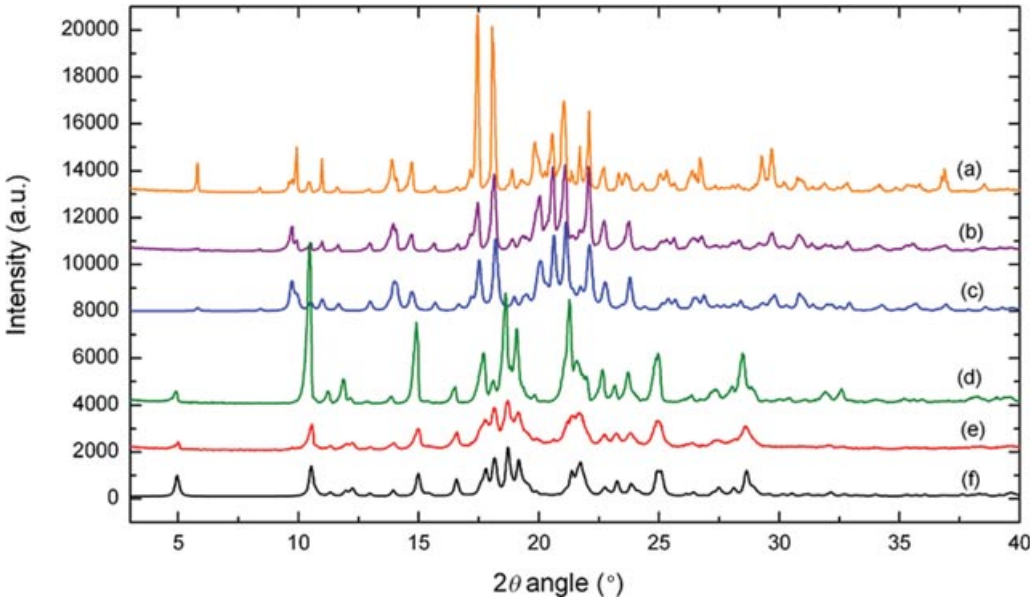

Figure 6. X-ray powder diffraction at room temperature for (a) observed form β (as grown), (b) observed form β (ground), (c) calculated form β, (d) observed form α (as grown), (e) observed form α (ground), and (f) calculated form α.

A decrease in the melting point after grinding is not new and has been observed in other compounds.[21]

The new exothermic event can be assigned to the crystallization of amorphous material induced by milling. The fact that grinding process is able to induce amorphous material is known[10,22] and is also consistent with the absence of any extra peaks in the XRPD results obtained from ground samples (see Fig. 6).

This new amorphous phase, obtained by grinding forms α and β, suffers a phase transition to crystallize in forms α and β, respectively. In our case, the amorphous substance is undergoing a first-order phase transition without nucleation because crystals of forms α and β are preexistent and are seeding the sample to address the transformation.

In order to progress in the study of seeding, a sample of form β with a barely detectable amount of form

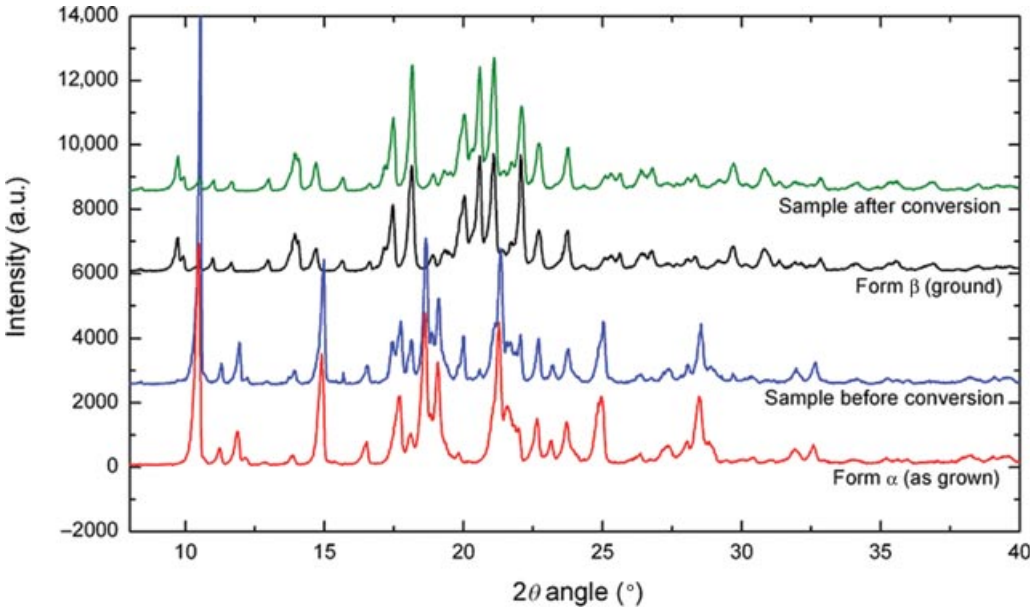

Figure 7. Slurry conversion process analyzed by X-ray powder diffraction at room temperature. Initial sample corresponds to a mixture of great amount of form α with a little content of form β, whereas final sample corresponds to pure form β.

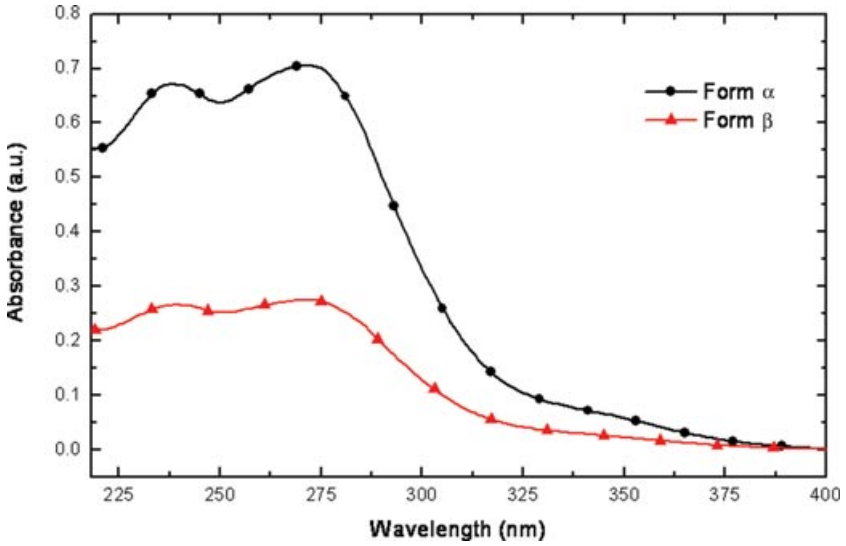

Figure 8. Ultraviolet–visible absorbance of form α (circles) and form β (triangles). Form α presents a solubility of about 2.5 times greater than form β.

α (see inset in Fig. 11) was also ground and analyzed (see Fig. 11). Although an amorphous phase is induced as a result of the grinding process, the thermal behavior seems to be rather different. The endothermic peak associated with the melting point of form α is present after and before grinding. However, the associated enthalpy is increased (see Table 5), which means an increment in the amount of form α in the sample. This increment could indicate the preference of the amorphous phase to crystallize in form α when this process is activated by temperature.

In order to study the time stability of the amorphous phase, a kinetic study at room temperature was performed, storing the ground samples for 1 week. In all cases it was observed that the amorphous phase was no longer present in any sample, which indicated that the amorphous phase had suffered a transition to another crystalline form. In those samples obtained by grinding form α, the presence of form β could be observed (see Fig. 9), whereas in the ones obtained by grinding form β, this polymorph was the only one detectable in the sample (see Fig. 10). This result provides an evidence to assert that the amorphous phase

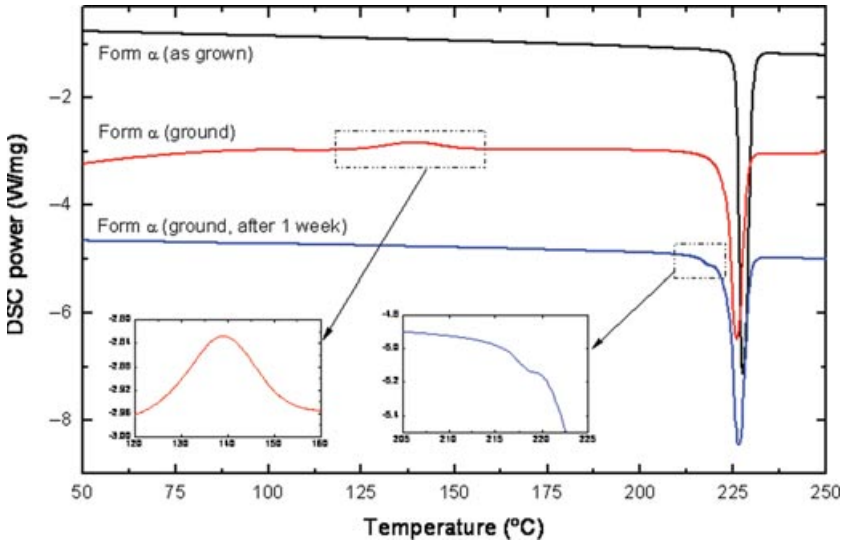

Figure 9. Characterization of the grinding effect on form α by differential scanning calorimetry (DSC) analysis. Ground sample presents a new thermal event characterized by exothermic peak at about 140°C; the melting point of form α has decreased from 226°C to 223°C. In ground sample, after 1 week aging, the exothermic peak is no longer present, but a little endothermic peak at about the melting point of form β is detectable.

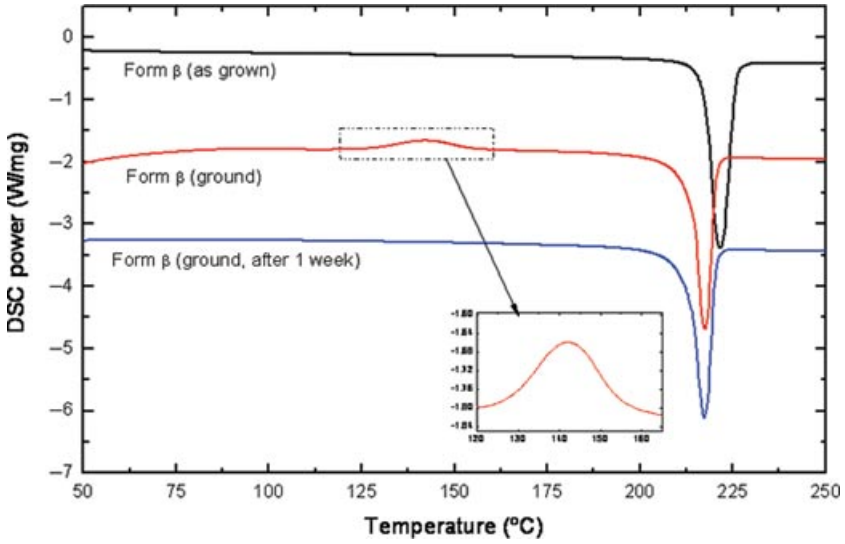

Figure 10. Characterization of the grinding effect on form β by differential scanning calorimetry (DSC) analysis. Ground sample also presents the exothermic peak at 140°C; the melting point of form β has also suffered a decrease from 217°C to 213°C. In ground sample, after 1 week aging, the exothermic peak is no longer present.

Table 5. Temperature and Enthalpy Associated to Each Thermal Event in the Traces Shown in Figures 9, 10, and 11

Thermal Event—Peak of Form α Name		T_{onset} [°C]	T_{peak} [°C]	Enthalpy [J/g]
Form α (Fig. 9)	As - grown	226	228	105.2
	Just ground	223	226	91.3
	Ground + 1 week aging	224	226	94.9
Form β (Fig. 10)	As - grown	–	–	–
	Just ground	–	–	–
	Ground + 1 week aging	–	–	–
Sample (Fig. 11)	As - grown	ND	228	0.3
	Just ground	224	226	2.7
	Ground + 1 week aging	ND	226	0.3
Thermal Event—Peak of Form β Name		T_{onset} [°C]	T_{peak} [°C]	Enthalpy [J/g]
Form α (Fig. 9)	As - grown	–	–	–
	Just ground	–	–	–
	Ground + 1 week aging	ND	218	1.0
Form β (Fig. 10)	As - grown	217	221	110.6
	Just ground	214	217	96.7
	Ground + 1 week aging	213	217	98.3
Sample (Fig. 11)	As - grown	216	221	113.1
	Just ground	213	217	88.7
	Ground + 1 week aging	213	217	101.8
Thermal Event—Peak of Amorphous Phase Name		T_{onset} [°C]	T_{peak} [°C]	Enthalpy [J/g]
Form α (Fig. 9)	As - grown	–	–	–
	Just ground	123	139	16.7
	Ground + 1 week aging	–	–	–
Form β (Fig. 10)	As - grown	–	–	–
	Just ground	125	142	19.1
	Ground + 1 week aging	–	–	–
Sample (Fig. 11)	As - grown	–	–	–
	Just ground	127	142	18.7
	Ground + 1 week aging	–	–	–

ND, not determined.

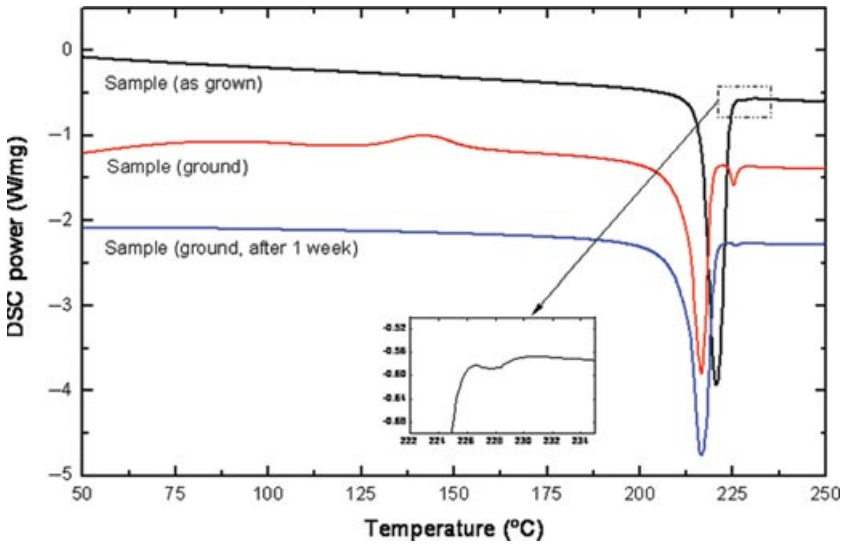

Figure 11. Characterization of the grinding effect on a sample by differential scanning calorimetry (DSC) analysis. The little endothermic peak at about the melting point of form α indicates that the sample contains a barely detectable amount of form α. Ground sample presents the exothermic peak at 140°C; the endothermic peak corresponding to the melting point of form α exhibits an increment in its enthalpy. The exothermic peak is no longer present in ground sample, after 1 week aging.

suffered a transition to form β with time at room temperature.

In order to determine the relation between grinding time and the amount of amorphous phase, samples were ground during 5, 20, and 40 min in a manual agate mortar. It was observed that the intensity of the exothermic peak rose with the grinding time, indicating increment of the amorphous phase content in the sample.

CONCLUSIONS

We have found conformational polymorphism in imatinib mesylate, where imatinib molecules generate C11—H11···O1 and C5—H5···N2 intramolecular H bond in forms α and β, respectively, and shown the main conformational differences in the values of torsion angles around N5—C12 and C4—C6 bonds. Even though the previously mentioned conformational differences, both crystal structures present a dimer-chain arrangement. Dimers are mainly determined by hydrogen bonding interactions and some weak π–π interactions, which produce extra cohesion. The connection between dimers is provided by mesylate ion via hydrogen bonding interactions. The neighboring chains are linked by very weak interactions: C—H···π interactions in form α and π–π interactions in form β.

We have to mention that at room temperature, thermal disorder was observed in the mesylate ion in form α, which could be removed at low temperatures (–123°C). This thermal disorder makes the bonding scheme between dimers—the basic structural unit—weaker. Subsequently, the observed disorder provides both a loosening of the low-temperature crystal bonding configuration and a high degree of molecular mobility, both of them precursor characteristics of a high energy material. This situation could be the reason for the tendency to generate an amorphous material by grinding.

We have proved by slurry conversion method and by relative solubility determinations that form β corresponds to the more stable crystalline form at room temperature. This is also in agreement with the fact that at room temperature, the mesylate ion is disordered in form α. Moreover, form α (the metastable polymorph at room temperature) presents higher melting point and greater enthalpy than form β (see Table 5). This case seems to bear an enantiotropic relationship between forms α and β, but the expected phase transition can be hindered due to conformational polymorphism.

The amorphous crystallization can be activated by both temperature or aging (time). As we have always been able to experience with impure amorphous material, importance of the role of seeding is shown when the recrystallization is activated by temperature. The amorphous substance obtained by grinding as grown samples of forms α and β recrystallizes in forms α and β, respectively. However, in the case of ground sample prepared from a mixture of forms α and β (even in the case of a low amount of form α), the amorphous phase crystallizes in form α, pointing out the possible preference of the amorphous material to crystallize in this form when the temperature is increased.

Conversely, when the amorphous crystallization is kinetically studied at room temperature, the amorphous phase crystallizes in form β after a week, showing that seeding is not important in this case and the amorphous material is able to form critical nuclei that continually grow into the matrix to produce form β.

ACKNOWLEDGMENTS

We acknowledge Consejo Nacional de Investigaciones Científicas y Técnicas for financial help (PIP 2009 0889), Agencia Nacional de Promoción Científica y Tecnológica for providing Gemini A diffractometer (project PME 01113), and Alicia Petragalli for her help in the XRPD experiments.

REFERENCES

1. Byrn SR. 1982. Solid state chemistry of drugs. New York: Academic Press.
2. Haleblian J, McCrone W. 1969. Pharmaceutical applications of polymorphism. J Pharm Sci 58:911–929.
3. Barrio M, Espeau P, Tamarit JL, Perrin MA, Veglio N, Ceolin R. 2009. Polymorphism of progesterone: Relative stabilities of the orthorhombic phases I and II inferred from topological and experimental pressure–temperature phase diagrams. J Pharm Sci 98:1657–1670.
4. Caira MR. 1998. Crystalline polymorphism of organic compounds. Top Curr Chem 198:163–208.
5. Sun CC. 2009. Materials science tetrahedron—A useful tool for pharmaceutical research and development. J Pharm Sci 98:1671–1687.
6. Brittain HG. 2002. Effects of mechanical processing on phase composition. J Pharm Sci 91:1573–1580.
7. Dunitz JD. 1995. Phase changes and chemical reactions in molecular crystals. Acta Cryst B 51:619–631.
8. Brittain HG. 1999. Effects of pharmaceutical processing on drug polymorphs and solvates (chapter 8). In Polymorphism in pharmaceutical solids; Brittain HG, Fiese EF, Eds. New York: Marcel Dekker, Inc.
9. Brittain HG. 2011. Polymorphism and solvatomorphism 2009. J Pharm Sci 100:1260–1279.
10. Bauer-Brandl A. 1996. Polymorphic transition of cimetidine during manufacture of solid dosage forms. Int J Pharm 140:195–206.
11. Ruscica R, Bianchi M, Quintero M, Martinez A, Vega DR. 2010. Solid state forms of zoledronic acid: Polymorphism in hydrates. J Pharm Sci 99:4962–4972.
12. Vega DR, Baggio R, Tombari D, Roca M. 2011. Aging driven decomposition in zolpidem hemitartrate hemihydrate and the single crystal structure of its decomposition products. J Pharm Sci 100:1377–1386.
13. Dulucq S, Krajinovic M, Takimoto CH, Calvo E. 2010. The pharmacogenetics of imatinib. Genome Med 2:85.
14. Takimoto CH, Calvo E. 2008. Principles of Oncologic Pharmacotherapy In Cancer management: A multidisciplinary approach. Pazdur R, Wagman LD, Camphausen KA, Hoskins WJ., Eds. UBM Medica, Norwalk, USA.
15. Patent WO99/03854, Patent US2008/0090833 A1 (April 17, 2008). Jegorov A, Chudik M, Aronhime J, Gavenda A, Faustmann J.
16. Patent US6,894,051 B1 (May 17, 2005). Zimmermann J, Sutter B, Burger HM.
17. CrysAlisPro Version 1.171.33.66. 2008. Oxford Diffraction Ltd. Blacksburg, Virginia.
18. Sheldrick GM. 2008. A short history of SHELX. Acta Cryst A 64:112–122
19. Farrugia LJ. 1999. WinGX. J Appl Cryst 32:837–838.
20. Allen FH. 2002. The Cambridge Structural Database: a quarter of a million crystal structures and rising Acta Cryst B 58:380–388.
21. Otsuka M, Masumoto T, Kaneniwa N. 1986. Effect of environmental temperature on polymorphic solid state transformation of indomethacin during grinding. Chem Pharm Bull 34:1784–1793.
22. Otsuka M, Kaneniwa N. 1984. Effect of grinding on the physiochemical properties of cephalexin powder. Chem Pharm Bull 32:1071–1079.